Journal of Alloys and Compounds 527 (2012) 48–52

Contents lists available at SciVerse ScienceDirect

Journal of Alloys and Compounds

journal homepage: www.elsevier.com/locate/jallcom

# Study of structural, electrical and magnetic properties of Zn doped $La_{0.67}Sr_{0.33}MnO_3$

Hilal Ahmed, Shakeel Khan*, Wasi Khan, Razia Nongjai, Imran Khan

*Department of Applied Physics, Z.H. College of Engineering & Technology, Aligarh Muslim University, Aligarh-202 002, India*

ARTICLE INFO

*Article history:*
Received 17 November 2011
Received in revised form 13 February 2012
Accepted 17 February 2012
Available online xxx

*Keywords:*
XRD
Magnetoresistance
Double-exchange interaction
Curie temperature

ABSTRACT

The structural, electrical and magnetic properties have been investigated on $La_{0.67}Sr_{0.33}Mn_{1-x}Zn_xO_3$ ($x = 0.1$ and 0.2) system. The samples have been prepared through the conventional solid-state reaction route. All the prepared samples were found in single phase with orthorhombic crystal structure. The crystallite sizes were estimated through X-ray diffraction (XRD) using the Debye–Scherrer's formula. Temperature dependent resistivity data shows metal to semiconducting (M–S) transition for both samples. Magnetization measurements confirm that the Curie-temperature ($T_C$) is found to decrease with Zn doping. The reduction in $T_C$ is attributed to the fact that the double-exchange interaction between $Mn^{3+}$–$O^{2-}$–$Mn^{4+}$ network has been destroyed by the substitution of Zn at Mn-site.



## 1. Introduction

The rare-earth doped manganites with the general formula of $R_{1-x}A_xMnO_3$ (R = Rare earth, A = divalent alkaline earth) have attracted much attention in the last decade or so, due to their unique and versatile properties, such as colossal magnetoresistance (CMR) [1,2], gas sensing [3] and fuel cell [4]. Nevertheless, several factors such as the requirement of large magnetic fields, to observe the CMR effect, make the realization of their full potential a rather slow process, and therefore, there are intensive efforts ongoing to optimize the properties of these manganites [5].

The physics of CMR is also closely related to the bad metal features which are ubiquitously observed in the conducting transition metal oxides with strong electron–electron (electron correlation) or electron–lattice interactions. The correlated electrons which are almost localized on the respective atomic sites bear three attributes, namely, charge, spin and orbital degrees of freedom [6,7]. The conduction electrons with an orbital degree of freedom (3d $e_g$ orbitals) are scattered not only by the strong electron-correlation effect but also by the strong electron–lattice coupling termed as Jahn–Teller interaction [8]. The collective or local Jahn–Teller (JT) distortions, as described by the displacement of the oxygen ions surrounding Mn sites, are observed everywhere when the compound shows the dramatic resistive (metal to semiconducting) or magnetic (antiferromagnetic to ferromagnetic) transitions.

The changing $Mn^{3+}/Mn^{4+}$ ratios in the CMR materials are essentially related to the doping mechanism to control the effective Mn valency [9,10]. This is achieved by either substitution and/or by changing overall oxygen contents, which determines the value of metal to semiconducting transition temperature, $T_P$. In addition, most of these compounds go through a structural phase transition often coupled with the para to ferromagnetic transition and accompanied with a change in sign of charge carriers at $T_P$ [11,12]. The static and dynamic magnetic properties of $LaMnO_{3+\delta}$ bulk and nanocrystalline materials were studied by Chandra et al. [13]. They observed ferromagnetic and antiferromagnetic phases coexisted in these samples. The nature of the ferromagnetic but insulating state for $0.1 < x < 0.17$ in $La_{1-x}Sr_xMnO_3$, and perhaps up to $x \sim 0.3$ for other narrower-W manganites (e.g. $Pr_{1-x}Ca_xMnO_3$), is still puzzling and under investigation. Unlike the other elements, e.g. Fe, Co, Ni and Cu, the mechanism of Zn doping at Mn site is different and only few reports on this system are available about the transport properties of bulk and thin films [14,15]. Some researchers observed the effect of Zn substitution on para to ferromagnetic transition temperature in $La_{0.67}Ca_{0.33}Mn_{1-x}Zn_xO_3$ [16,17]. Whereas, Ghosh et al. [18] studied the effects of transition elements (Cr, Fe, Co, Ni, Cu, Zn) doping in $La_{0.7}Ca_{0.3}MnO_3$ for a fixed (5% at Mn site) dopant concentration. These authors pointed out metal–insulator transition temperature, the Curie temperature, and the maximum value of magnetoresistance (MR), with respect to lattice parameter and the ionic radii of dopants.

The partial substitution of $Zn^{2+}$ at the magnetic sublattice of mixed-valent manganese in $La_{0.6}Sr_{0.4}MnO_3$ induces a random potential fluctuation because the $Zn^{2+}$ ion has the completely filled

* Corresponding author. Tel.: +91 571 2700920x3035; fax: +91 571 2700042.
*E-mail address:* skhanapd@gmail.com (S. Khan).

0925-8388/$ – see front matter © 2012 Elsevier B.V. All rights reserved.
doi:10.1016/j.jallcom.2012.02.110

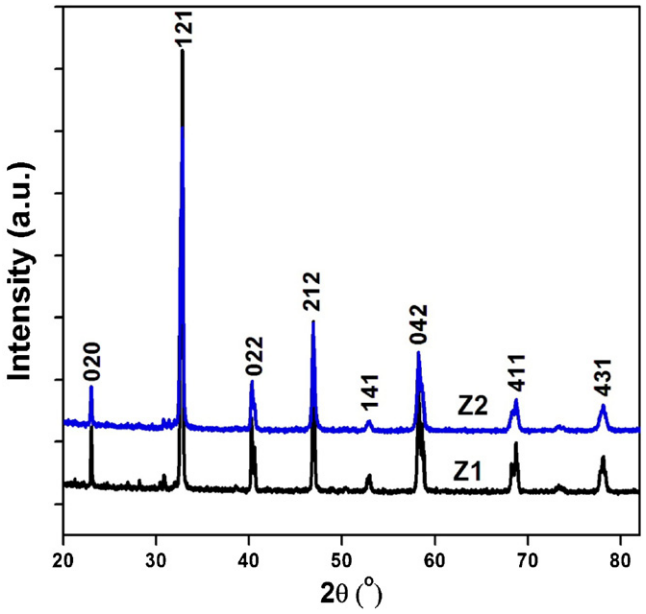


**Fig. 1.** XRD patterns of Z1 and Z2 samples.

$3d^{10}$ electronic configurations, which is different from those of $Mn^{3+}$ and $Mn^{4+}$ configuration respectively. Secondly, the $Zn^{2+}$ ions do not carry any magnetic moment as they are also expected not to participate in the ferromagnetic (FM) interaction and hence dilute the magnetic sublattice [19]. Keeping this in view, we have aimed to study the structural, electrical and magnetic properties of zinc doped manganites. In this paper, we have carried out the comparative studies of 10 and 20% zinc doping at the Mn site in $La_{0.67}Sr_{0.33}MnO_3$ (LSMO), i.e. $La_{0.67}Sr_{0.33}Mn_{0.9}Zn_{0.1}O_3$ (onwards mentioned as Z1) and $La_{0.67}Sr_{0.33}Mn_{0.8}Zn_{0.2}O_3$ (onwards mentioned as Z2) systems using the resistivity and magnetization measurements. We observed a considerable change in the metal to semiconducting (M–S) transition temperature ($T_P$) and Curie-temperature ($T_C$) with Zn doping.

## 2. Experimental details

The $La_2O_3$, $SrCO_3$, $MnO_2$ and ZnO materials were taken as 2.6810, 1.1967, 1.9216 and 0.2007 g respectively for 10% Zn doped sample, while for 20% doped sample these amounts were 2.6868, 1.1993, 1.7117 and 0.4022 g respectively. The polycrystalline bulk samples of $La_{0.67}Sr_{0.33}Mn_{0.9}Zn_{0.1}O_3$ (Z1) and $La_{0.67}Sr_{0.33}Mn_{0.8}Zn_{0.2}O_3$ (Z2) were prepared by mixing and grinding of ingredients $La_2O_3$, $SrCO_3$, $MnO_2$ and ZnO powders (all of AR-grade with purity > 99.9% and purchased from CDH) in stoichiometric ratio, heated at 1000 °C for 12 h [7,20]. After this heat treatment samples were ground thoroughly in agate mortar and again heated at 1250 °C for 24 h. For final preparation, samples were ground with polyvinyl alcohol (PVA), pelletized and calcined at 1300 °C for 24 h.

All the samples were characterized by X-ray diffraction (XRD) (Bruker D8 Advance) using Cu-$K_\alpha$ radiation ($\lambda \sim 1.5406$ Å) in the $2\theta$ range 20–80° with scan speed 0.2°/min and step size is 0.02°. The resistivity of samples was measured by using standard four-probe technique in the temperature range 5–300 K in a cryostat assembly (VTI or magnet system). Four contacts of indium were made on a well sintered pellet using conductive solder of low melting point. Fine enameled copper wires were used to pass the constant current of the order of few microamperes through the outer two leads using a constant current source (KEITHLY, Model-2400). The voltage developed across the two inner leads was measured using the sensitive digital multimeter (KEITHLY, Model-182) as a function of temperature. The temperature was controlled using the temperature controller (Lakeshore-DRC-93CA). The magnetization measurements were carried out using Vibrating Sample Magnetometer (VSM, Model-MTS-XL) in the temperature range 100–400 K.

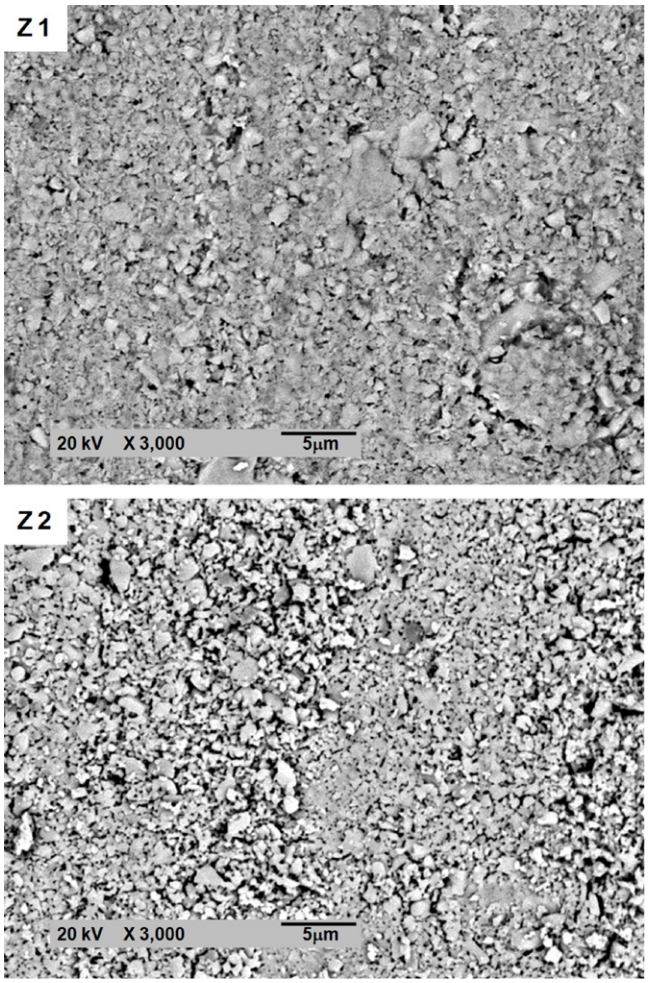


**Fig. 2.** SEM micrographs of Z1 and Z2 samples.

## 3. Results and discussion

### 3.1. Surface and morphological studies

The representative XRD patterns of Z1 and Z2 are shown in Fig. 1. At room temperature, the XRD patterns show that both the samples are formed in a single phase with orthorhombic crystal symmetry with *Pnma* space group.

Average crystallite size using most intense peak (1 2 1) has been determined from XRD patterns by using Debye–Scherrer's formula [21,22]. The unit cell volume increases with increase in Zn concentration, since the ionic radius of $Zn^{2+}$ is larger than that of $Mn^{3+}$, so the Zn substitution can of course make the volume larger as the doping level goes from 10% to 20%. The lattice parameters, unit cell volumes and the crystallite size have been tabulated in Table 1. The lattice parameters changed considerably as compared to parent compound LSMO. The as-obtained crystallite sizes ($D$) are 27.48 nm and 24.32 nm for the samples Z1 and Z2 respectively.

SEM micrographs for Z1 and Z2 samples are displayed in Fig. 2. The particles can be clearly distinguished and all the observed particles connect with each other. The particles of the sample Z2 are in better and clear shape than those of the Z1 sample, revealing that increase in Zn doping could improve the crystallization of the sample. In addition, the particle sizes for the two samples are comparable, which are estimated to be mostly within 200 nm range. Obviously, the particle sizes observed by SEM are several times larger than the crystallite sizes calculated by XRD [23].

**Table 1**
Lattice parameters, unit cell volume and crystallite size for Z1 and Z2 samples.

| Sample | Symmetry | Lattice parameters | | | Unit cell volume (Å$^3$) | Crystallite size (nm) |
|---|---|---|---|---|---|---|
| | | $a$ (Å) | $b$ (Å) | $c$ (Å) | | |
| Z1 | Orthorhombic | 5.742 | 7.668 | 5.532 | 243.5720 | 27.48 |
| Z2 | Orthorhombic | 5.537 | 7.695 | 5.743 | 244.6932 | 24.32 |

### 3.2. Electrical transport properties

Fig. 3(a) and (b) shows the temperature dependence of resistivity for both the samples Z1 and Z2, which exhibit metal-semiconducting (M–S) transition. The M–S transition temperature ($T_P$) decreases with increase in Zn concentration. The observed values of $T_P$ for doped LSMO are lower than that of undoped sample (LSMO) which is 295 K near room temperature, reported elsewhere [24]. It is also observed that resistivity drops with the application of magnetic fields from 0.734 Ω-cm at 0 T to 0.369 Ω-cm at 5 T for 10% zinc doped sample while from $4.75 \times 10^4$ Ω-cm at 0 T to $4.45 \times 10^3$ Ω-cm at 5 Tesla for 20% zinc doped sample at $T_P$. The value of $T_P$ and the resistivity of doped samples show the dramatic change as the concentration goes from 10% to 20%. The values of $T_P$ for 10% and 20% Zn doped samples are shown in Table 2 at different fields. Table 2 also exhibits the resistivity obtained at zero field and $T = T_C/2$, where $T_C$ is the Curie temperature of sample. The doped samples have higher resistivity than undoped LSMO at zero field and $T = T_C/2$ ($\rho \sim 4.92 \times 10^{-3}$ Ω-cm). These results are predicted due to the fact that the destruction of the partial double exchange interaction would lead to a decrease of the electrons' hopping at Mn-site substitution [25].

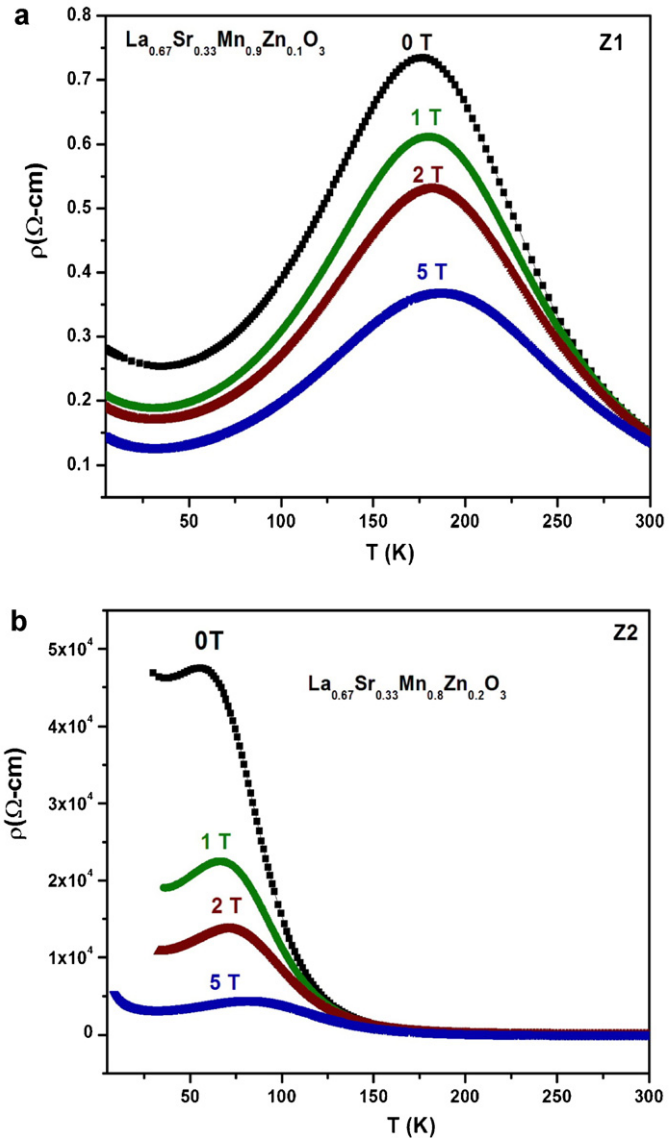


**Fig. 3.** Temperature dependence of resistivity for (a) Z1 and (b) Z2 samples.

**Table 2**
Transport and magnetic parameters.

| Sample | $T_P$ (K) | | | | $T_C$ (K) | $\rho^a$ (Ω-cm) |
|---|---|---|---|---|---|---|
| | (0 T) | (1 T) | (2 T) | (5 T) | | |
| Z1 | 176.88 | 180.08 | 182.29 | 186.94 | 316.88 | 0.7 |
| Z2 | 57.14 | 66.82 | 70.89 | 81.67 | 315.46 | 1009 |

[a] At $T = T_C/2$ and zero field.

It is well known that the resistivity is mostly influenced by the presence of grain boundaries which act as a region of enhanced scattering for the conduction electrons [24]. Moreover, the resistivity in a magnetic field is smaller than that in zero field. The alignment of the core spin of Mn ions under the applied magnetic field can cause the reduction in the spin scattering of the itinerant electrons. As a result the resistivity should decrease with increasing the magnitude of the applied magnetic field. In Fig. 3(a) and (b) the peak of M–S transition can be seen. Since the M–S transition is closely correlated with the FM transition, the position of the peak has same tendency as $T_C$ in doped samples. The tendency of the magnetic field to stabilize the FM state moves the M–S peak to the high temperature region [25].

### 3.3. Magnetoresistance

The CMR as a function of temperature, calculated using the formula $(\rho_H - \rho_o/\rho_H)$ (here $\rho_H$ and $\rho_o$ are the values of resistivity in the presence and absence of magnetic field) are shown in Fig. 4(a) and (b). In Fig. 4(a) with $x = 0.1$, MR peaks can be observed in the vicinity of experimental temperature range where the sample exhibits an M–S transition. Furthermore, a significant MR ratio appears in the low-temperature range, either metallic or insulating, and decreases monotonically with increasing temperature. It is noteworthy that the hump in the MR peaks is increasing with the increasing magnetic fields. In Fig. 4(b), the CMR effect can be visualized only up to 150 K. The encircled portion of the figure indicates that the large MR difference can be clearly seen within the range 35–85 K at different fields. The MR values at different temperatures and different fields are displayed in Table 3. The presence of magnetically disordered regions increasingly affects the zero field resistivity $\rho_o$. This together with the change of resistivity ($\Delta\rho$) induced by applied field decreases due to the broadening of ferromagnetic transition, leading to the reduction in CMR ratio.

### 3.4. Magnetic properties

Fig. 5 shows the temperature dependence of dc-magnetization ($M$–$T$) of the Z1 and Z2 samples measured in a field of 5000 Oe

**Table 3**
MR ratio at different temperatures and fields.

| Sample | MR% | | | | | | | | |
|---|---|---|---|---|---|---|---|---|---|
| | 1 T | | | 2 T | | | 5 T | | |
| | 35 K | 150 K | 300 K | 35 K | 150 K | 300 K | 35 K | 150 K | 300 K |
| Z1 | −34.49 | −23.64 | 0.41 | −49.11 | −42.97 | −2.89 | −97.21 | −106.64 | −12.79 |
| Z2 | −131.04 | −13.70 | 0 | −326.15 | −13.70 | 0 | −1337.18 | −55.09 | 0 |

during the warming process from 100 K to 400 K. The inset of this figure shows the temperature dependent dc-susceptibility ($\chi$–$T$) for both samples. The Curie temperature ($T_C$) values, determined from the maximum point in the d$M$/d$T$ or d$\chi$/d$T$ are listed in Table 2. For the undoped LSMO sample, the $T_C$ is 365 K [25]. These results are quite different as compared to the result observed by Markovich et al. [26]. There is a monotonous decrease in $T_C$ with increasing zinc concentration. For the samples with $x = 0.1$ and 0.2, the paramagnetic (PM) state to FM state transition is narrow. This fact indicates a wider distribution of the magnetic exchange interactions in the Mn–O network. Moreover, for the Z1 and Z2 samples, a magnetization drop appears at certain low temperatures in the $M$–$T$ curve. The reduction in $T_C$ is also because of the fact that the double-exchange interaction between $Mn^{3+}$–$O^{2-}$–$Mn^{4+}$ network has been destroyed by the substitution of dopants at Mn-site. It is also noteworthy that the increasing doping level leads to the more drop off of $T_C$.

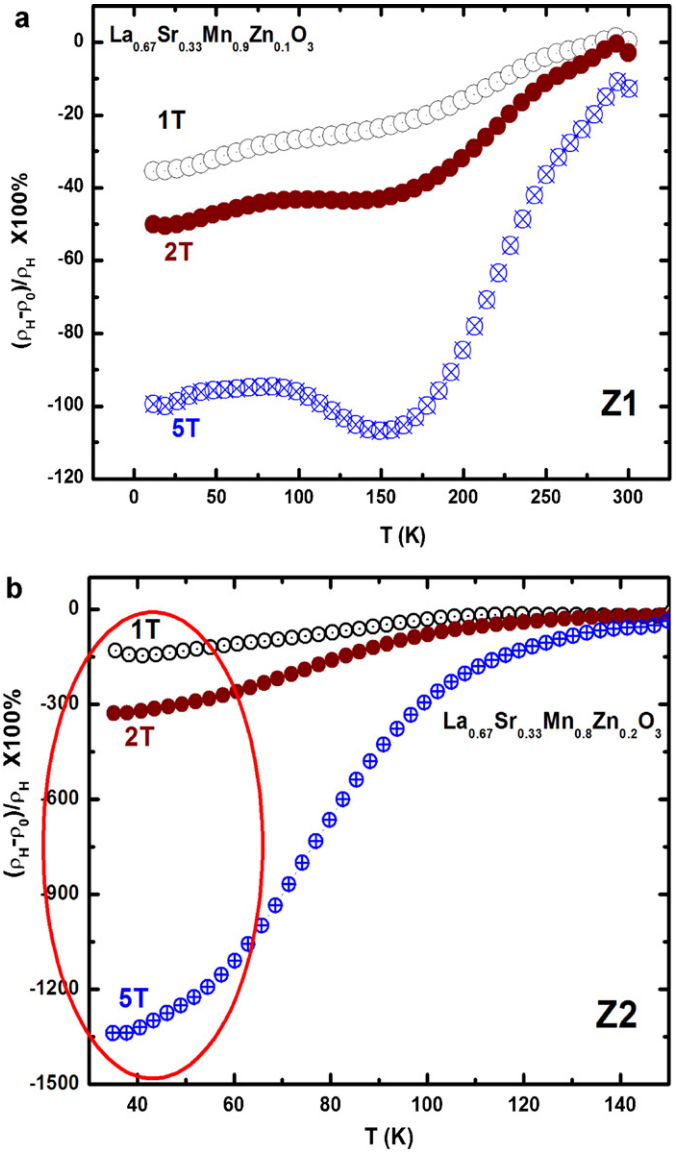


**Fig. 4.** Magneto-resistances of (a) Z1 and (b) Z2 samples.

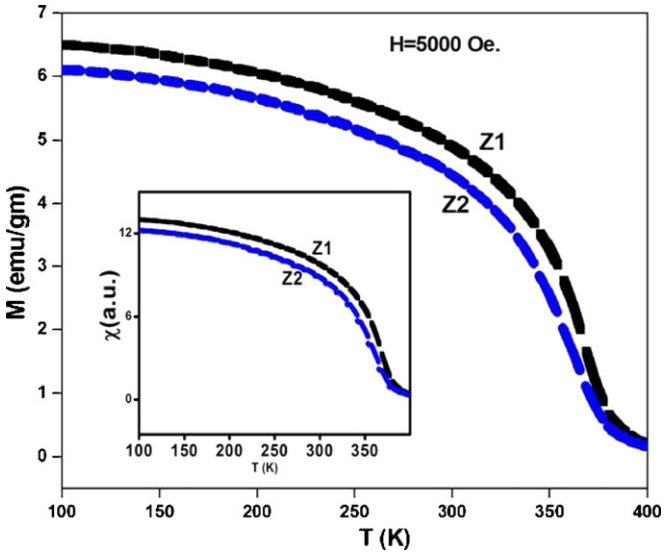


**Fig. 5.** $M$–$T$ curve for Z1 and Z2 samples. The inset shows d.c. susceptibility for the same.

## 4. Conclusions

In summary, the structural, electrical transport and magnetic properties of Zn doped $La_{0.67}Sr_{0.33}MnO_3$ samples were studied. XRD patterns confirm that the Zn ions are successfully substituted at Mn site. The resistivity data shows that both sample show metal to semiconducting (M–S) transition and the M–S transition temperature is shifted towards the higher temperature value with the effect of increasing magnetic field for both samples. The magnetoresistance is found to be negative in the entire temperature range for the Z1 sample except at 300 K (1 T) while for sample Z2 it can be seen only up to 150 K. Zn substitution on Mn site leads to a strong decrease of the Curie temperature because of suppression of ferromagnetism.

## Acknowledgments

The authors are thankful to University Grants Commission (UGC) New Delhi, India for financial support. Authors are also grateful to the Professor Ajay Gupta and Dr. Rajeev Rawat, UGC-DAE CSR, Indore, India for encouragement and providing experimental facilities.

## References


[1] Q.X. Song, N. Liu, G.Q. Yan, W. Tong, Y. Sun, J. Rare Earths 24 (3) (2006) 332.
[2] C. Mitra, P. Raychaudhuri, J. John, S.K. Dhar, A.K. Nigam, R. Pinto, J. Appl. Phys. 89 (2001) 524.
[3] P. Raychaudhuri, S. Mukherjee, A.K. Nigam, J. John, U.D. Vaisnav, R. Pinto, P. Mandal, J. Appl. Phys. 86 (1999) 5718.
[4] Z. Jiang, Z. Lei, B. Ding, C. Xia, F. Zhao, F. Chen, Int. J. Hydrogen Energy 35 (2010) 8322.
[5] J. Gao, S.Y. Dai, T.K. Li, Phys. Rev. B 67 (2003) 153403.
[6] Y. Tokura, Phys. Today 56 (2003) 50.
[7] G.H. Jonker, J.H. van Santen, Physica 16 (1950) 337.
[8] L. Pinsard, J. Rodriguez-Carvajal, A. Revcolevschi, J. Alloys Compd. 262–263 (1997) 152.
[9] G.O. Siqueira, R.M. Belardi, P.H. Almeida, C.L. da Silva, M.C. Brant, T. Matencio, R.Z. Domingues, J. Alloys Compd. http://dx.doi.org/10.1016/j.jallcom.2012.01.023, 2012.
[10] K. Cherif, S. Zemni, Ja. Dhahri, Je. Dhahri, M. Oumezzine, M. Ghedira, H. Vincent, J. Alloys Compd. 396 (2005) 29.
[11] G. Kartopu, M. Es-Souni, J. Appl. Phys. 99 (2006) 033501.
[12] P. Fleming, R.A. Farrell, J.D. Holmes, M.A. Morris, J. Am. Ceram. Soc. 93 (4) (2010) 1187.
[13] S. Chandra, A.I. Figueroa, B. Ghosh, M.H. Phan, H. Srikanth, A.K. Raychaudhuri, J. Appl. Phys. 109 (2011) 07D720.
[14] T. Atsumi, N. Kamegashira, J. Alloys Compd. 25 (1997) 161.
[15] S.T. Liu, Y. Wu, Y.Q. Jia, J. Alloys Compd. 197 (1993) 91.
[16] Z. Shenggui, C. Changle, J. Kexin, J. Rare Earths 25 (2007) 734.
[17] V.P.S. Awana, E. Schmitt, E. Gmelin, A. Gupta, A. Sedky, A.V. Narlikar, O.F. de Lima, C.A. Cardoso, S.K. Malik, W.B. Yelon, J. Appl. Phys. 87 (2000) 5034.
[18] K. Ghosh, S.B. Ogale, R. Ramesh, R.L. Greene, T. Venkatesan, K.M. Gapchup, R. Bathe, S.I. Patil, Phys. Rev. B 59 (1999) 533.
[19] K. Vijayanandhini, T.R.N. Kutty, Solid State Commun. 141 (2007) 252.
[20] P. Mandal, S. Das, Phys. Rev. B 56 (1997) 15073.
[21] P. Scherrer, Gottinger Nachrichten Gesell 2 (1918) 98.
[22] M.A.M. Khan, M. Wasi Khan, M. Alhoshan, M.S. AlSalhi, A.S. Aldwayyan, M. Zulfequar, J. Alloys Compd. 503 (2010) 397.
[23] C. Vazquez-Vazquez, M.C. Blanco, M.A. Lopez-Quintela, R.D. Sanchez, J. Rivas, S.B. Oseroff, J. Mater. Chem. 8 (1998) 991.
[24] P. Van Cuong, J. Dho, H. Yeol Park, D.H. Kim, Appl. Phys. A 95 (2009) 567.
[25] X. Chen, Z. Wang, J. Cai, B. Shen, W. Zhan, J. Chen, J. Appl. Phys. 86 (1999) 4535.
[26] V. Markovich, E. Rozenberg, G. Gorodetsky, D. Mogilyansky, B. Revzin, J. Pelleg, J. Appl. Phys. 90 (2001) 2347.